Developmental Biology 384 (2013) 290–300

Contents lists available at ScienceDirect

Developmental Biology

journal homepage: www.elsevier.com/locate/developmentalbiology

Sequential effects of *spadetail*, *one-eyed pinhead* and *no tail* on midline convergence of nephric primordia during zebrafish embryogenesis

Chiu-Ju Huang [a,b], Val Wilson [a], Sari Pennings [a], Calum A. MacRae [b], John Mullins [a,*]

[a] British Heart Foundation Centre for Cardiovascular Science, University of Edinburgh, QMRI, 47 Little France Crescent, Edinburgh, EH16 4TJ, United Kingdom
[b] Brigham and Women's Hospital and Harvard Medical School, 75 Francis Street, Boston, MA 02115, USA

ARTICLE INFO

Article history:
Received 18 May 2012
Received in revised form
12 June 2013
Accepted 5 July 2013
Available online 13 July 2013

Keywords:
Pronephric kidney
Midline convergence
Kidney fusion

ABSTRACT

Midline convergence of organ primordia is an important mechanism that shapes the vertebrate body plan. Here, we focus on the morphogenetic movements of pronephric glomerular primordia (PGP) occurring during zebrafish embryonic kidney development. To characterize the process of PGP midline convergence, we used *Wilms' tumour 1a* (*wt1a*) as a marker to label kidney primordia, and performed quantitative analyses of the migration of the bilateral PGP. The PGP initially are approximately 350 μm apart in a wild type embryo at 10 h post fertilization (hpf). The inter-PGP distance decreases exponentially between 10 and 48 hpf, while the anterior–posterior (*A–P*) dimension of each PGP increases linearly between 10 and 12 hpf, then decreases substantially between 12 and 24 hpf. Using mutants in the Nodal receptor cofactor *one-eyed pinhead* (*oep*) and the T-box transcription factors *spadetail* (*spt*) and *no tail* (*ntl*), we were able to define distinctive regulation underlying these sequential phases of PGP midline migration. Zygotic *oep* mutants ($Zoep^{-/-}$) exhibited defects in midline convergence after 16 hpf. *Spt* is necessary for PGP convergence from 10 hpf, whereas *ntl*'s effect on convergence does not begin until 24 hpf. Notably, we observed normal cardiac convergence in $spt^{-/-}$ and $ntl^{-/-}$ embryos implying that these novel roles of *spt* and *ntl* in PGP migration cannot be explained simply by generalised effects on midline convergence. These findings demonstrate that quantitative approaches to developmental migration allow the parsing of early patterning events, and in this instance suggest that the zebrafish may offer insights into midline urogenital migration anomalies in humans.

Introduction

Midline convergence of organ primordia is an important mechanism in the patterning of mesodermal (Sakaguchi et al., 2006) and endodermal structures (Ober et al., 2004). Noncanonical *Wnt* signalling has been shown to regulate midline convergence of organ primordia during zebrafish development (Matsui et al., 2005). In contrast with the zebrafish kidney, the development of the mammalian kidney results in bilateral structures for the pronephros and mesonephros, without midline convergence. In zebrafish (*Danio rerio*), the adult kidney consists of two distinct lobes. The anterior lobe, situated at the cranial aspect of the swim bladder, is commonly referred to as the head kidney or pronephros. The posterior lobe of the kidney is located between the vertebral column and the swim bladder, and is named the posterior/trunk kidney or mesonephros. The head kidney takes the form of a transversely placed tissue mass that lies across the midline (Hall et al., 2007; Hsu et al., 2003), potentially resembling intermediate forms of renal patterning observed in higher organisms (O'Brien et al., 2008; Oktem et al., 2008). Previous work has identified commonalities of gene expression between the developing zebrafish pronephros and mammalian kidney primordia (Bouchard et al., 2002; Rackley et al., 1993; Serluca and Fishman, 2001; Wingert and Davidson, 2008). We hypothesized that distinctive mechanisms underlie discrete steps in the midline convergence of PGP in zebrafish, and that understanding the molecular basis of these events might offer insights into the midline fusion and other migratory abnormalities that are observed in abnormal mammalian urogenital development (O'Brien et al., 2008).

At early developmental stages, the head kidney in zebrafish consists of a single nephron, with a fused glomerular mass at the midline. A pair of tubules runs laterally from the glomerulus and connects to the bilateral pronephric ducts (Drummond et al., 1998). This fused single glomerulus, which can be observed from 48 h post fertilization (hpf), originally develops from the bilateral intermediate mesoderm at 13 hpf (Serluca and Fishman, 2001), implicating midline convergence in pronephric-glomerular (PG) morphogenesis in zebrafish.

The specification of the intermediate mesoderm occurs many hours before the formation of the fused glomerulus (48 hpf) during embryogenesis. During this time, not only does convergence occur,

* Corresponding author. Fax: +44 131 242 6782.
E-mail address: jmullins@ed.ac.uk (J. Mullins).

0012-1606/$ - see front matter © 2013 Published by Elsevier Inc.
http://dx.doi.org/10.1016/j.ydbio.2013.07.002

but there is also continued differentiation of the PGP and coalescence of these cells into a functioning glomerulus. To characterize the kinetics of PG morphogenesis in greater detail, we devised a simple approach to the quantitative analysis of PGP coalescence and migration. We used *Wilms' tumour 1a* (*wt1a*) as a marker to label bilateral PGP, and then measured the distance between bilateral PGP to determine rates of convergence as well as parallel changes in the anterior–posterior (*A–P*) dimensions of the PGP (coalescence). Two additional podocyte markers, *nephrin* (*nph*) and *podocin* (*pod*), encoding key molecules required to maintain the filtration barrier of the foot processes of podocytes (Nilius et al., 2007), were used to verify the differentiation status of cells within the PGP.

To test our hypothesis we studied PGP morphogenesis in 3 existing zebrafish mutants: zygotic *one-eyed pinhead* (*Zoep*), *spadetail* (*spt/tbx16*), and *no tail* (*ntl*), chosen on the basis of the importance of these genes in cell adhesion and migration, as well as for their known effects on tissues surrounding the PGP (Supplementary, Fig. S1). Oep is an EGF related protein, a cofactor in Nodal signalling (Gritsman et al., 1999; Shen and Schier, 2000; Yeo and Whitman, 2001), and is essential for the formation of all endodermal and several mesodermal tissues (Feldman et al., 2000, 1998; Schier and Shen, 2000). Both *spt* and *ntl* are T-box transcription factors (*T-box*). *spt* regulates the cell adhesion molecule paraxial protocadherin, during the movement of somite progenitors and subsequent somitogenesis (Amacher and Kimmel, 1998; Ho and Kane, 1990; Kimmel et al., 1989; Weinberg et al., 1996; Yamamoto et al., 1998). It is also a key mediator of FGF signalling in the formation of trunk mesoderm (Griffin et al., 1998). *ntl* is the zebrafish homologue of the mouse *brachyury* gene, which is required for notochord formation (Odenthal et al., 1996a; Schulte-Merker et al., 1994).

Our results show that in wild type (WT) zebrafish embryos, whole mount *in situ* (WISH) and simple quantitation of the morphological dynamics of the PGP allow the definition of discrete phases of PGP midline convergence. The three phases we are able to define are; specification between 10 and 12 hpf, coalescence between 12 and 24 hpf, and fusion between 24 to 48 hpf. $Zoep^{-/-}$ embryos exhibit defects in convergence after 16 hpf (coalescence phase) but not in shortening the length of the PGP, suggesting separate regulation for these contemporaneous cell movements. *ntl* is required only after 24 hpf which is beginning of the fusion phase, whereas *spt* appears to play major roles in the midline convergence of the PGP, since the the specification phase. The expression of markers of the differentiated PGP, *podocin* and *nephrin,* was normal in these mutant embryos, further supporting the discrete regulation of PGP convergence and differentiation. Notably, we observed normal cardiac midline convergence in $spt^{-/-}$ and $ntl^{-/-}$ embryos demonstrating that the *T-box* genes, *spt* and *ntl* are specifically required for the midline convergence of PGP. Convolution of pronephric tubules was abnormal in $spt^{-/-}$ embryos. Lack of convoluted tubule marker expression in $Zoep^{-/-}$ embryos was regardless severity of PGP phenotypes. Together our findings demonstrate that the regulation of pronephric glomerular formation requires the orchestration of multiple discrete cell movements in addition to differentiation, and that each of these events has specific molecular requirements. These findings also suggest that systematic quantitative approaches to developmental biology can also yield important information.

Materials and methods

Zebrafish strains and maintenance

zebrafish (*D. rerio*) mutant alleles, oep^{tz57} (Zhang et al., 1998), spt^{b104} (Griffin et al., 1998), ntl^{tc41} (Odenthal et al., 1996b), ntl^{b195} (Schulte-Merker et al., 1994) were studied. Wild-type fish were AB strain. Zebrafish genomic DNA was extracted from 2 mm^2 caudal fin clips (Altschmied et al., 1997). Polymerase chain reaction (PCR) was used to identify the following alleles in heterozygous adult fish. The reverse primers, oeptz57R (5′-CTC ACC CGA ACA GTT GAC TCG TCA C) and ntltc41R (5′-GTG TAT CCT GGG TTC GTA TTT GTG CT) are specific to the oep^{tz57}- and ntl^{tc41}-alleles, respectively. The primer pair, sptF (5′-TTG ACC ACA ATC CCT TTG CCA A) and spt104R (5′-GCC TTC ACC TCC AGC TCT TTA CG), flank the deletion found in spt^{b104} and amplify approximately 0.9 kb and 1.9 kb products in the mutant and WT, respectively. Fish were maintained as described in The Zebrafish Book (Westerfield, 1995). Embryos were staged according to (Kimmel et al., 1995) by hours post-fertilization (hpf). Between 10 and 18 hpf, embryo stage was determined by counting somites (Kimmel et al., 1995). Somite counting was confirmed by *wt1a* double *in situ* with *myod* in a different color. Staging of $spt^{-/-}$ embryos was determined from the siblings. Beyond 18 hpf, somite number is not easy to count and is closely related to hours post-fertilization, and so for embryos older than 18 hpf stage determination was based purely on the maintenance conditions (28.5 °C).

Whole-mount in situ hybridization (WISH)

Zebrafish embryos were incubated in 0.003% phenylthiourea to prevent pigment formation until the required developmental stage. After dechorionation, embryos were fixed in 4% paraformaldehyde overnight at 4 °C. The embryos were dehydrated in 100% methanol and stored at −20 °C at least 16 h prior to proceeding with whole mount *in situ* hybridization. Digoxigenin (DIG), or fluorescein labelled anti-sense RNA probe was generated by *in vitro* transcription (DIG/fluorescein RNA Labeling Kit, Roche). The probes synthesized for *wt1a*, *myod*, *oep*, *mibp2*, *cmlc2*, *nph*, *pod*, *nkx2.5 and slc20a1* covered the sequence regions of AF144550 (1274-871), NM_131262 (714-203), NM_131092 (480-1), NM_198877 (919-202), AF425743 (587-26), AY956356 (1147-693), NM_001040687 (782-291), NM_131421 (533-1043) and NM_213179 (685-106), respectively. WISH was performed according to standard protocols (Jowett, 2001). Alkaline phosphatase conjugated antibody (Roche) was used for the detection of DIG- (1:5000) or fluorescein-labelled (1:4000) compounds. Embryos were stained in the dark in AP buffer containing 0.1 to 0.16 mg/ml BCIP (5-bromo-4-chloro-3-indolyl phosphate, Roche) and 0.125 mg/ml NBT (nitro blue tetrazolium, Roche) for purple or BCIP and 0.2 mg/ml INT (iodonitrotetrazolium chloride, Sigma) for orange–brown. The whole-mount embryos were then stored in 4% PFA at 4 °C prior to imaging.

Imaging

A Leica M2 16F microscope with Leica LED 1000 modular daylight illumination (ring-light) and Leica DFC (300 FX) camera system were used to obtain images of embryos after whole-mount *in situ* hybridization. Individual embryos were embedded in 3% methylcellulose (400cP, Sigma) in glass bottomed culture dishes (FluoroDish™, 35 mm, 10 mm well, World Precision Instruments).

Measuring PG convergence and coalescence

PGP areas were identified by *wt1a* WISH (NBT/BCIP or NBT/INT staining). The WISH images were imported into GIMP (open source at www.gimp.org). The inter PGP distance and the *A–P* length of the PGP (Fig. 2A) were measured in pixels by using the Ellipse Select Tool. The pixels for the distance and length of PGP were converted into micrometers (μm) using a 0.1 mm stage graticule. These measurements were converted and compiled in Excel (Microsoft).

Statistical analysis and curve fitting

Mean and standard deviation (SD) of the measurements of each group were calculated. In the results section, the inter PGP distance

and the *A–P* length of the PGP were presented as observed mean ± SD. The scatter plot and trend line tool in Excel were used to generated the exponential, linear and quadratic functions in Fig. 2B and Fig. 6D. Fig. 2C was generated using the scatter plot function with data points connected by smoothened lines. Statistical analysis for the inter PGP distance and *A–P* length of the PGP between WT and mutants was performed by using the Student's *t*-test. A p value < 0.05 was considered as statistically significant. Bonferroni's correction for multiple testing was applied.

Morpholino injections

Morpholinos (MO) were obtained from Gene Tools, LLC. Stock solution for each MO is 1 mM in nuclease-free water. Injection mix consisted diluted MO, 1 × Danieau solution and 0.05% Phenol Red. About 5 nl of 0.1 mM *ntl* MO or mix of 0.4 mM *spt* MO1 and 0.1 mM *spt* MO2 was injected to 1- to 4-cell stage embryos. The MO sequences were: ntl MO, 5′GAC TTG AGG CAG GCA TAT TTC CGA T (Nasevicius and Ekker, 2000); *spt* MO1, 5′AGC CTG CAT TAT TTA GCC TTC TCT A; spt MO2, 5′GAT GTC CTC TAA AAG AAA ATG TCA G (Lewis and Eisen, 2004).

Results

Midline convergence underlies pronephros morphogenesis

In zebrafish, two homologues of the Wilms' tumour gene, *wt1a* and *wt1b*, have been identified with slightly divergent expression patterns (Bollig et al., 2006). *wt1a* is a marker that during development becomes restricted to the bilateral PGP and specifies the cells forming the glomerulus. Downregulation of this zinc-finger transcription factor results in absence of glomeruli (Perner et al., 2007).

wt1a-expressing cells were detected initially at 10 hpf (Fig. 1B; compared to no signal at 8 hpf Fig. 1A) and located bilaterally at a distance from the adaxial cells labelled by *myod* expression. Within an hour, *wt1a*-expression becomes more extensive and the expression pattern expands along the anterior–posterior (*A–P*) axis. The distance between the bilateral *wt1a*-expressing fields also narrows progressively during development (Fig. 1C). At 12 hpf, *wt1a*-expressing cells are arranged in two long strips adjacent to somites 1–5 bilaterally (Fig. 1D). These strips shorten substantially in the *A–P* dimension by 15 hpf (Fig. 1E) and exhibit faint and dense signal on the anterior and posterior side, respectively. Contrast of the faint and dense *wt1a* signal is even greater at

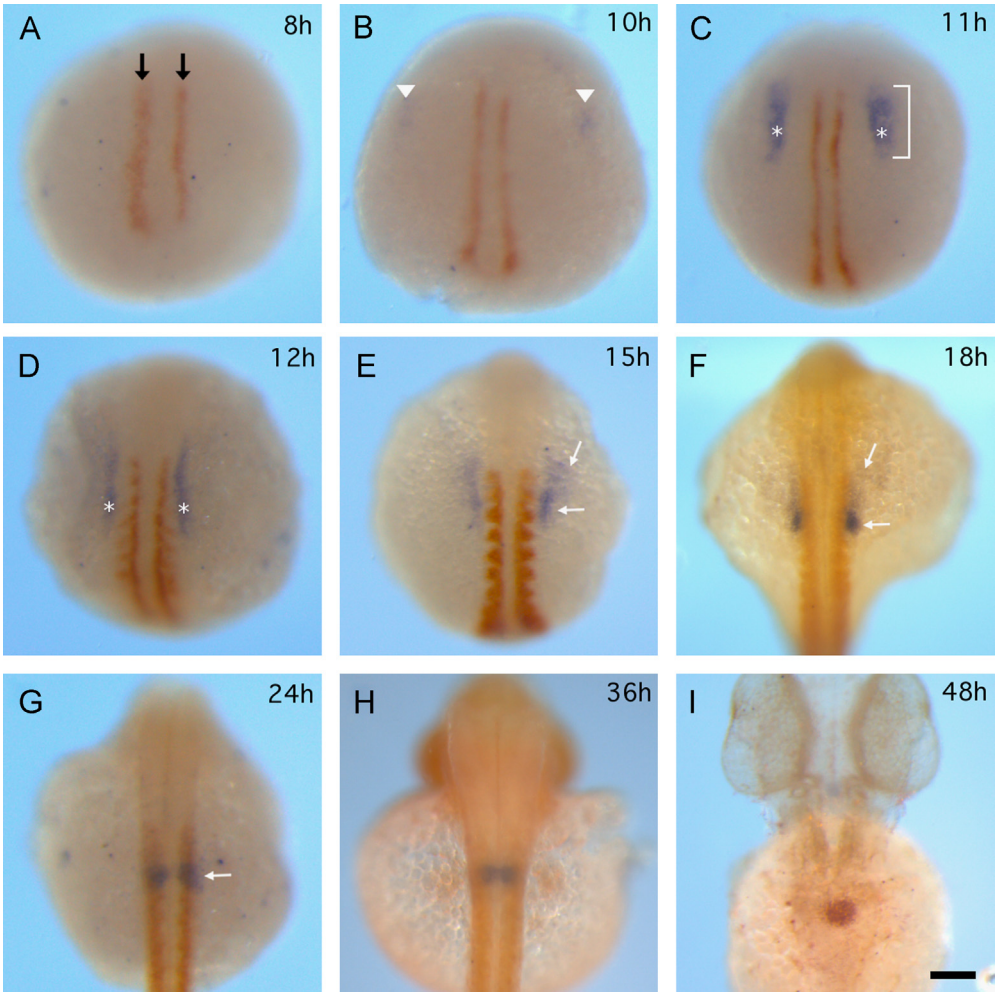

Fig. 1. Morphogenetic changes of PGP during 8–48 hpf development. Dynamic *wt1a* expression (blue) in relation to somite morphogenesis (*myoD* expression, orange–brown) at 8, 10, 11, 12, 15, 18, 24 hpf is shown in (A)–(G). (A) *MyoD* expression labels adaxial cells at 8 hpf (black arrow). (B) Initial *wt1a* expression (arrowhead) locates bilaterally at a distance from the adaxial cells. ((C) and (D)) *Wt1a* expression pattern expands along the (A)–(P) dimension (bracket). *Wt1a* expression crosses on left–right axis at third somite were the measure points for inter distance of PGP (asterisks). ((E) and (F)) White arrows indicate faint (anterior side) and dense (posterior side) signal in *wt1a*-positive cells. (G) The faint signal is almost unseen and *wt1a*-positive cells become compact round shape (white arrow). (H) The bilateral PGP (blue) adjacent to each other at 36 hpf, *myoD* and *mibp2* were stained orange–brown. (I) A single fuse PGP (orange–brown) appears in midline at 48 hpf. All images are dorsal view and at the same magnification. The scale bar in H indicates 100 μm.

18 hpf (Fig. 1F). After 24 hpf *wt1a* expression is restricted to the PGP as described previously (Drummond et al., 1998). By 48 hpf, the two PGP have converged and fused at the midline (Figs. 1G–I). The dynamic expression pattern of *wt1a* over time 10 to 48 hpf is summarized in Fig. 2A.

Quantification of pronephros morphogenesis

The midline convergence process labeled by *wt1a* WISH exhibited a series of complex changes during development between 10 and 48 hpf. In order to better define the events during midline convergence we quantitated the morphogenetic behaviours of the bilateral PGP. The inter-PGP distance and the length (anterior–posterior dimensions) of the PGP were measured at 10, 11, 12, 15, 16, 18, 24, 36 and 48 hpf and plotted (Figs. 2B and C). The maximum inter-PGP distance is 330 ± 31 μm at 10 hpf and the minimum is 7 ± 6 μm at 48 hpf. Curve fitting of the series of inter PGP measurements demonstrates an exponential reduction between 10 and 48 hpf (Fig. 2B). The length of the PGP, by contrast, is initially 90 ± 30 μm, and increases linearly by 12 hpf (Fig. 2C). Between 12 and 24 hpf the PGP length decreases from 196 ± 14 to 52 ± 9 μm. The length of the PGP is 48 ± 5 μm at 36 hpf and 52 ± 5 μm at 48 hpf. Based on the quantitative (Fig. 2B) analysis and *wt1a* WISH images (Fig. 1), the morphogenesis of the PGP can be partitioned into three distinct phases, outlined in Fig. 2A: specification, coalescence, and fusion. In the specification phase, as defined by wt1a expression, at 10–12 hpf, the distribution of PGP cells expands along the *A–P* axis (Figs. 1B–D, Fig. 2C). After the initial wave of specification, during the coalescence phase, *wt1a*-expressing domains differentiate into faint anterior and dense posterior sides (Figs. 1E and F), which eventually shorten their length along the *A–P* axis (Fig. 2C) and restrict to compact round areas (Fig. 1G). In the fusion phase, between 24 and 48 hpf, the two PGP converge towards each other and fuse at the midline (Fig. 1G–I, Fig. 2C).

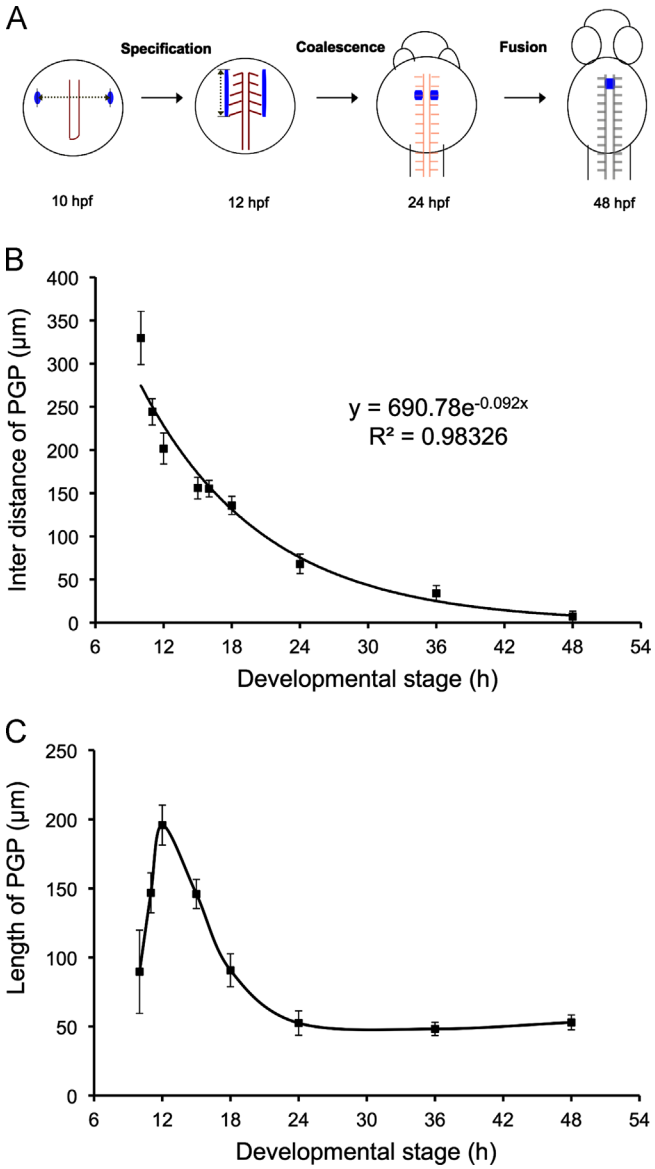

Fig. 2. The inter distance and length of PGP. (A) Cartoon summary of PG (blue) morphogenesis indicates distinct morphogenetic changes between 10 and 48 hpf. The method to measure points for the inter distance and length of PGP is also shown in this panel. (B) Scatter plot of inter distance of PGP for a series of developmental stages, 10 ($n=12$), 11 ($n=38$), 12 ($n=30$), 15 ($n=24$), 16 ($n=18$), 18 ($n=30$), 24 ($n=26$), 36 ($n=16$), 48 ($n=33$) hpf. The curve fitting and *R*-squared value are displayed on the right-hand corner. (C) The plot of of PGP length for a series of developmental stages, 10 ($n=11$), 11 ($n=37$), 12 ($n=22$), 15 ($n=24$), 18 ($n=30$, 24 ($n=21$), 36 ($n=16$), 48 ($n=32$) hpf. Error bars represent SD.

Discrete mechanisms for differentiation and midline convergence of the PGP

Double WISH of *wt1a* and *myoD* showed a normal PGP pattern at 12 hpf (Fig. 3A), evidence of normal PGP specification in *Zoep*$^{-/-}$. A compact round *wt1a* expression pattern was observed at 24 hpf regardless of subsequent normal (Fig. 3B; arrows) or abnormal midline convergence (Fig. 3D; arrows), suggesting that the mechanisms for *A–P* morphological change are independent from those regulating midline convergence. There was significant variability in the severity of the convergence defect observed at 48 hpf (Figs. 3C and E; arrows).

To examine the effect of *Zoep* on PGP midline convergence in more detail, the inter-PGP distance was measured at 12, 16, 24, 36 and 48 hpf in *Zoep*$^{-/-}$ embryos and compared with WT (Fig. 3F). The inter-PGP distance at 12 hpf in *Zoep*$^{-/-}$ embryos (196 ± 15 μm) is similar to WT ($p=0.15$), but differences begin to emerge by 16 hpf. The inter-PGP distance was greater in *Zoep*$^{-/-}$ embryos (163 ± 11 μm, $p < 0.05$) than in WT (155 ± 10 μm). Large variation in inter-PGP distance was observed in *Zoep*$^{-/-}$ embryos and this was highly significant compared to WT at 24 hpf (138 ± 35 μm, $p < 0.0005$), 36 hpf (106 ± 48 μm, $p < 0.0005$) and 48 hpf (153 ± 39 μm, $p < 0.0005$). These results suggest that *Zoep* affects PGP midline convergence in the coalescence phase and that the effect progress through the fusion phase.

Zoep$^{-/-}$ embryos were further evaluated using WISH with additional markers of kidney morphogenesis. Nephrin or podocin are required to maintain the filtration barrier formed by the foot processes of podocytes (Nilius et al., 2007). In zebrafish *nephrosis 1, congenital, Finnish type (nephrin)-like* (*nph/nphs1l*) and *nephrosis 2, idiopathic, steroid-resistant* (*podocin, pod/nphs2*), are first expressed exclusively in the PGP at 24 hpf (Kramer-Zucker et al., 2005). The expression of *nph* and *pod* is not affected in *Zoep*$^{-/-}$ embryos at 36 hpf when compared to WT embryos (Fig. 4A–C), irrespective of whether the defect in midline convergence is mild (with PGP inter-distance 41 to 53 μm, Fig. 4D–F) or severe (with PGP inter-distance 151 to 162 μm, Fig. 4G–I). These results strongly suggest that initial PGP specification and differentiation are discretely regulated from PGP midline convergence.

T-box genes play roles in PGP midline convergence

The *T-box* genes, *ntl* and *spt/tbx16,* are key genetic factors in notochord and somite formation, respectively (Odenthal et al.,

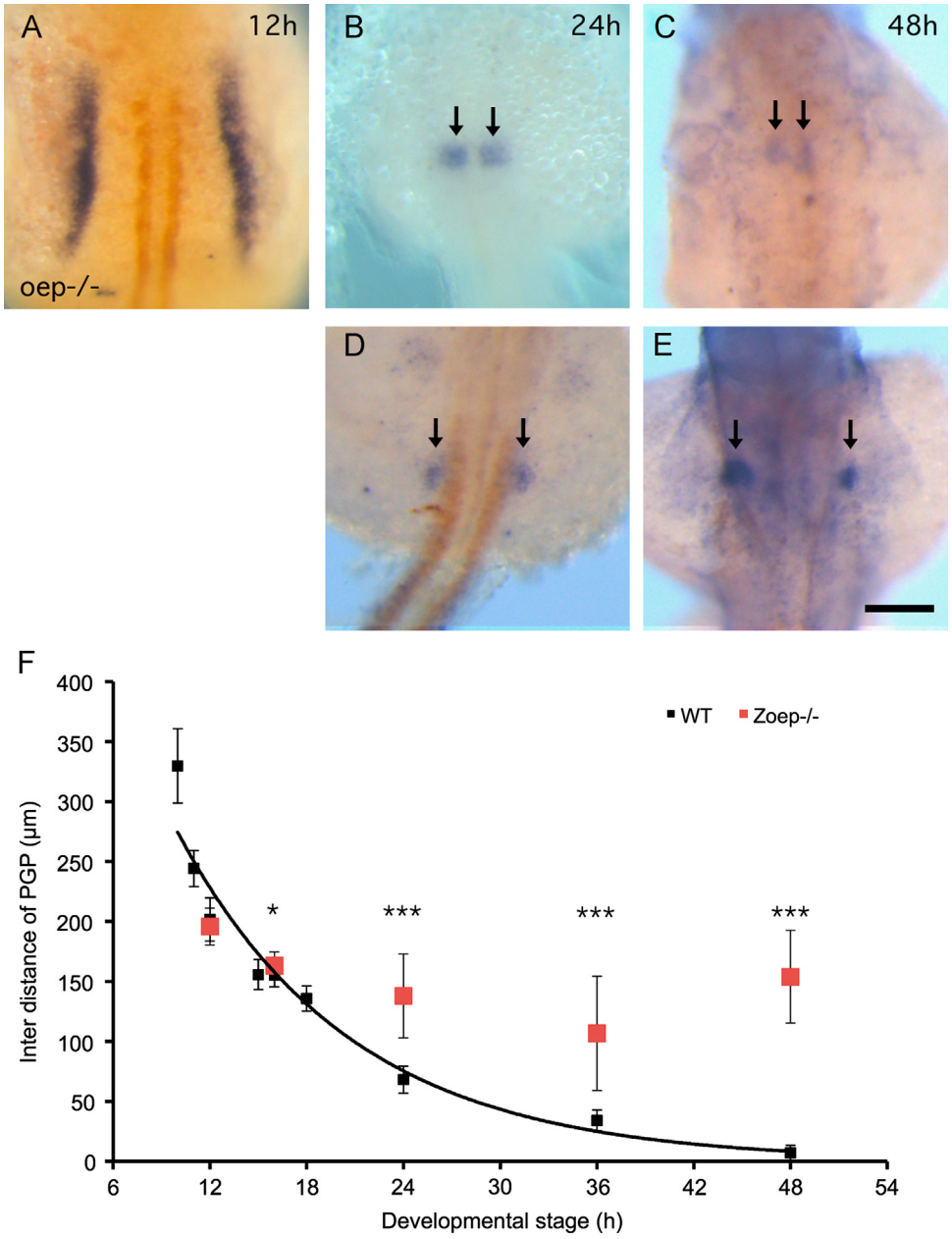

Fig. 3. Varied PGP phenotypes in Z*oep*$^{-/-}$ embryos. (A) *Wt1a* (blue) and *myoD* (orange) double *in situ* shows normal PG pattern at 12 hpf (6-somite) in Z*oep*$^{-/-}$embryos. Both normal (B) and abnormal (D) PG (arrows) phenotype is observed at 24 hpf. Mild (C) and severe PG (arrows) midline convergence defect is observed at 48 hpf. All images are dorsal view anterior to the top and at the same magnification. The scale bar in E indicates 100 μm. (F) Z*oep*$^{-/-}$ inter distance of PGP (red squres) is compare to WT on it's plot at 12 (n=40, P=0.15), 16 (n=24), 24 (n=22), 36 (n=34), 48 (n=29) hpf. $P<0.05$, *$P<0.0005$, ***Error bars represent SD.

1996a; Weinberg et al., 1996). Z*oep* genetically interacts with these two genes in the formation of somitic mesoderm (Griffin and Kimelman, 2002; Schier et al., 1997). We explored the effect of surrounding tissue formation (Supplementary, Fig. S1) on PGP midline convergence in *ntl*$^{-/-}$ and *spt*$^{-/-}$ embryos.

We initially compared *wt1a* expression pattern between *ntl*$^{-/-}$ and WT at 12 (Fig. 5A, Fig. 1D), 24 (Fig. 5B, Fig. 1G) and 48 hpf (Fig. 5C, Fig. 1I). There was no noticeable difference between *ntl*$^{-/-}$ and WT at 12 and 24 hpf on the images. At 48 hpf fused PGP was not formed in *ntl*$^{-/-}$ embryos (Fig. 5C). We next quantified and analyzed WISH results at 11, 12, 24, 36 and 48 hpf. There was no significant difference in the inter-PGP distance between *ntl*$^{-/-}$ and WT embryos at 11 (242 ± 15 μm, $p=0.68$) and 12 hpf (207 ± 13 μm, $p=0.29$). While at 24 hpf the inter PGP distance in *ntl*$^{-/-}$ embryos is slightly greater than WT (81 ± 11 μm, $p<0.0005$), the difference between *ntl*$^{-/-}$ and WT is also significant at 36 hpf (81 ± 8 μm, $p<0.0005$) and 48 hpf (48 ± 16 μm, $p<0.0005$). These data imply that *ntl* does not affect PGP midline convergence until the fusion phase.

In contrast to the observations in *ntl*$^{-/-}$ embryos, from our WISH results it is evident that PGP convergence is abnormal in *spt*$^{-/-}$ from a very early stage (Fig. 6A–C). The distance between the bilateral PGP remains constant at 12, 24 and 48 hpf in *spt*$^{-/-}$ embryos, with no suggestion of any convergence movement. Furthermore, the *wt1a* expression domain was restricted to a much smaller area at 12 hpf in *spt*$^{-/-}$ embryos (Fig. 6A). The shape of the PGP was irregular in *spt*$^{-/-}$ embryos at 24 and 48 hpf (Fig. 6B and C) compared to that in WT embryos (Fig. 1G and I). We quantified the inter-PGP distance in *spt*$^{-/-}$ embryos at 11, 12, 15, 16, 24 and 48 hpf and plotted the results (Fig. 6D). In contrast to the exponential decrease in inter-PGP distance from 11 hpf (245 ± 13 μm) to 48 hpf (7 ± 6 μm) in WT embryos, the

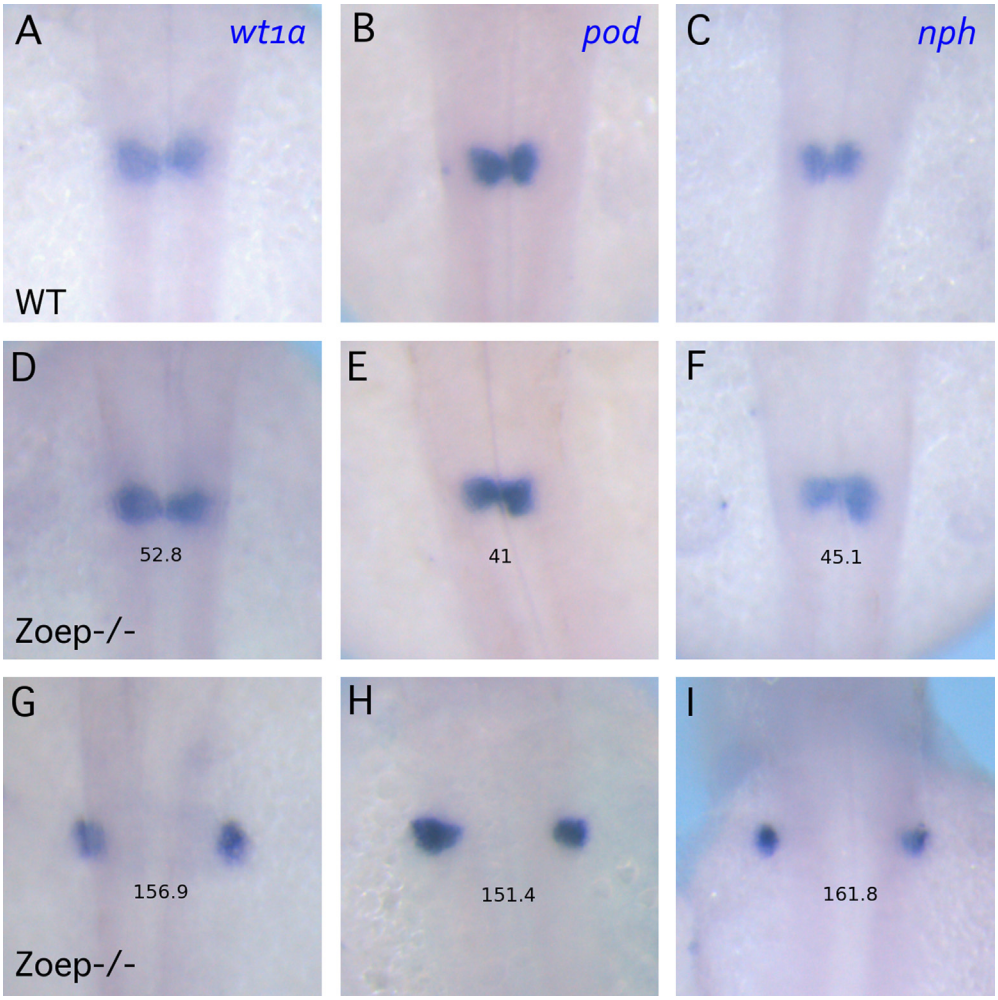

Fig. 4. PGP differentiation in *Zoep*$^{-/-}$ embryos. Whole-mount *in situ* hybridization of *wt1a* ((A), (D), (G)), *podocin* ((B), (E), (H)) or *nephrin* ((C), (F), (I)) was stained blue in WT ((A)–(C)) and *Zoep*$^{-/-}$ ((D)–(I)) embryos at 36 hpf. The numbers (μm) on Zoep$^{-/-}$ embryos ((D)–(I)) indicate the inter distance (μm) of PGP. All images are dorsal view anterior to the top and at the same magnification.

changes in inter-PGP distance in *spt*$^{-/-}$ embryos were subtle from 11 hpf (142 ± 12 μm) to 48 hpf (103 ± 16 μm). The dynamic behavior of the inter PGP distance between 11 and 48 hpf can be fitted to a simple quadratic function with $R^2 = 0.9828$ (Fig. 6 D) with a minimum inter-PGP distance of 78 μm at 33.5 hpf (Fig. 6D; arrow) and divergence after 33.5 hpf.

Expression of podocyte markers, *pod* (Fig. 8A–C) and *nph* (Fig. 8D–F) was normal in *ntl* (Fig. 8B and E; arrowhead) and *spt* morphant embryos (Fig. 8C and F; arrowhead). These results confirm a discrete mechanism for differentiation and midline convergence of PGP.

PGP, cardiac midline convergence, and tubule formation are dissociated

We also investigated PGP midline convergence in relation to the neighbouring anterior and posterior tissues: the heart and the tubule primordia (Serluca and Fishman, 2001). Double WISH of *nkx2.5* and *wt1a* in 12 hpf WT embryos showed that the heart primordia (Fig. 7A and B; red) are close to anterior intermediate mesoderm (Fig. 7A and B; blue) but, by 18 hpf the heart primordia have diverged from PGP (Fig. 7C). WISH of *cmlc2* was used to detect the cardiac morphogenesis phenotypes in *Zoep*$^{-/-}$, *spt*$^{-/-}$, *ntl*$^{-/-}$ and WT embryos. Similar to the varying severities of PGP defects in *Zoep*$^{-/-}$ embryos (Fig. 4D–I), convergence of the cardiac primordia also varied in these mutants (Fig. 7E and F) at 36 hpf. However, neither *spt*$^{-/-}$ nor *ntl*$^{-/-}$ ever exhibited a defect in cardiac convergence (Fig. 7H and I), despite clear effects on PGP convergence in the same embryos at 48 hpf.

The proximal convoluted tubule marker *slc20a1* was used to examine tubule structure in morpholino injected or mutant embryos and compared to WT at 48 hpf (Fig. 8). The paired convoluted tubules construct a funnel-like shape in WT embryos (Fig. 8A and D; arrows) with the anterior ends of the tubules on either side of the fused PGP. There is no notable tubule phenotype in *ntl* morphant embryos (Fig. 8B and E). The tubules remain posterior to the PGP and parallel to each other (Fig. 8C and F; arrows) in *spt* morphants. *slc20a1* expression is greatly reduced in Zoep$^{-/-}$ embryos, regardless of the severity of the PGP phenotypes (Fig. 8G–I; arrows). This faint *slc20a1* signal is similar to that observed in the poorly convoluted tubules in *spt* morphants.

Discussion

A systematic approach to uncover the networks regulating PGP convergence

A wealth of zebrafish mutants has been generated by chemical or retroviral mutagenesis (Amsterdam et al., 2004; Haffter et al., 1996). This has resulted in the identification of several mutants with PGP midline convergence defects. In *floating head* (*flh*), *sonic*

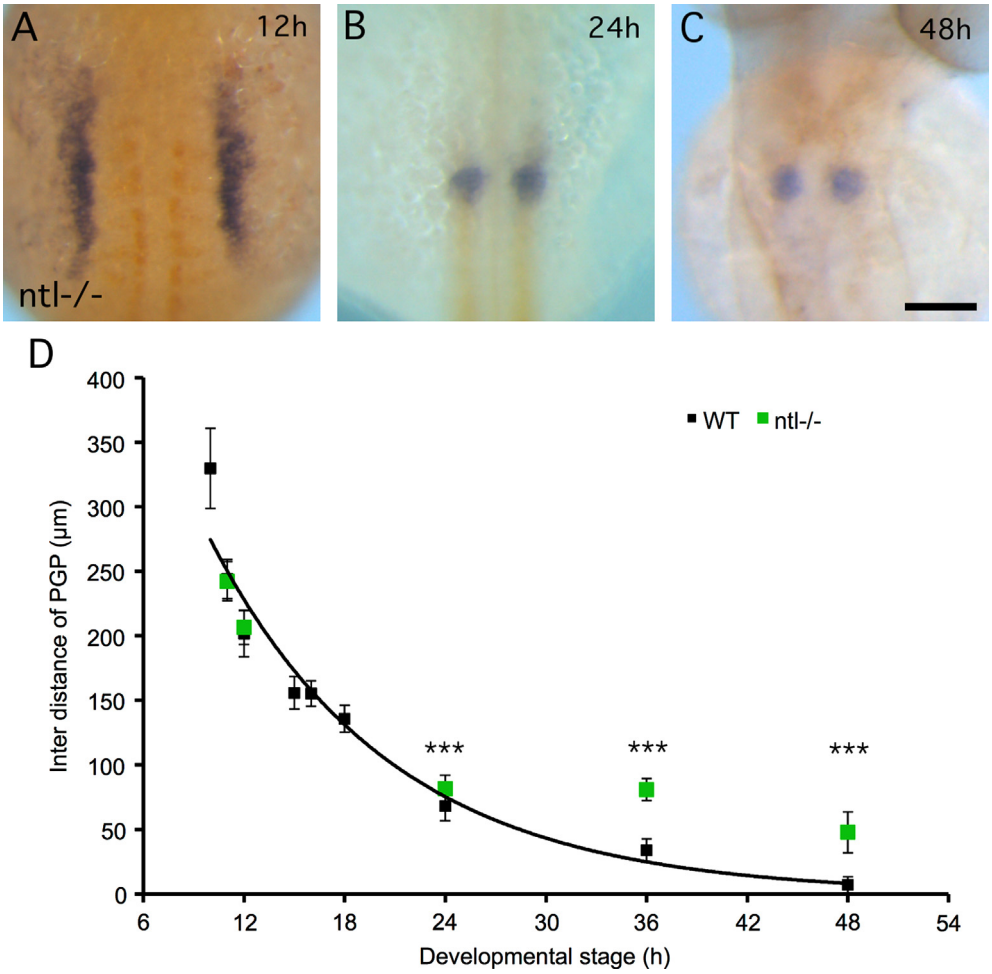

Fig. 5. PGP midline convergence phenotypes in $ntl^{-/-}$ embryos. ((A)–(E)) Whole-mount *in situ* hybridization of *wt1a* and *myoD* was stained blue and orange, respectively in 12 (A), 24 (B) and 48 hpf (C) $ntl^{-/-}$ embryos. The scale bar indicates 100 μm; ((A)–(C)) are at the same magnification. All images are dorsal view anterior to the top. (D) Quantification of convergence morphogenetic movements in $ntl^{-/-}$ embryos and comparison with WT. The inter distance of PGP was measured at 11 ($n=20$, $P=0.68$), 12 ($n=17$, $P=0.27$), 24 ($n=23$,), 36 ($n=29$), 48 ($n=20$) hpf. The inter distance of PGP is significant difference between $ntl^{-/-}$ and WT at 24, 36 and 48 hpf ($^{***}P<0.0005$). Error bars represent SD.

you (*syu*), and *you-too* (*yot*) mutants, glomeruli differentiate at ectopic lateral positions suggesting that midline signals are required for formation of the fused central glomus but not for the differentiation of functional glomeruli (Liu et al., 2000; Majumdar and Drummond, 2000). *Matrix metalloproteinase-2* (*MMP-2*) is thought to relay hemodynamic forces, via endothelial signaling, to direct the formation of the midline pronephric glomerulus. Mutants with impaired circulation, such as *island beat (isl), valentine (vtn),* and *silent heart (sih),* exhibit bilateral pronephric glomeruli (Serluca et al., 2002). In this study, we explore midline convergence phenotypes in *spt* and *ntl* mutants (Figs. 5 and 6), and add these two genes to the list of genetic factors required for PGP midline convergence. PGP convergence at the midline is necessary in order to connect with the dorsal aorta and circulation and is vital for functional kidney development (Drummond, 2003). Hence, a detailed understanding of the cellular dynamics of organogenesis is important to dissect the distinctive mechanisms of cell migration, differentiation and function during development.

A previous study of the origin of glomerular precursors (Serluca and Fishman, 2001) demonstrated that *wt1a* expression is a reliable marker of PGP during development. Simple quantitation of the dimensions of the PGP (*wt1a* expressing cells), and their subsequent convergence and shortening offers insights into the discrete regulation of the requisite developmental steps between 10 and 48 hpf (Fig. 1, Fig. 2A). Interestingly, there is already some evidence from the literature to support distinct stages during PGP morphogenesis. *wt1a*-expressing cells are not formed in $Zoep^{-/-}$; $spt^{-/-}$ double mutant embryos (Weidinger et al., 2002) indicating redundant roles for these genes in the initial formation of PGP precursors. Further, $kohtalo^{-/-}$ mutants exhibit persistent extended bilateral narrow strips of *wt1a*-expressing cells at 24 hpf (Hong et al., 2005), indicating an important role for *med12* in the coalescence step.

Our results suggest parallel mechanisms of PGP movement and differentiation in the progress of midline convergence. $Zoep^{-/-}$ embryos exhibit normal condensation of PGP length (Figs. 3A and B) and podocyte differentiation (Fig. 4) despite the defects in convergence prior to the fusion step (Figs. 3C and D). *oep* is mainly expressed in notochord and ventral mesoderm at these stages of embryogenesis (data not shown). *ntl* mutants, which lack midline *oep* expression (Schafer et al., 2005), display abnormal fusion but normal convergence (Fig. 5); hence notochord-specific expression of *oep* is not necessary for PGP midline convergence prior to fusion, suggesting that ventral mesoderm expressed *oep* may be required for midline convergence after 16 hpf. In addition, PGP convergence abnormalities appear after the initial specification step in $spt^{-/-}$ embryos (Fig. 6). The three genetic factors important for PGP midline convergence, *Zoep*, *spt* and *ntl*, appear to regulate discrete cellular mechanisms, the final effects of which

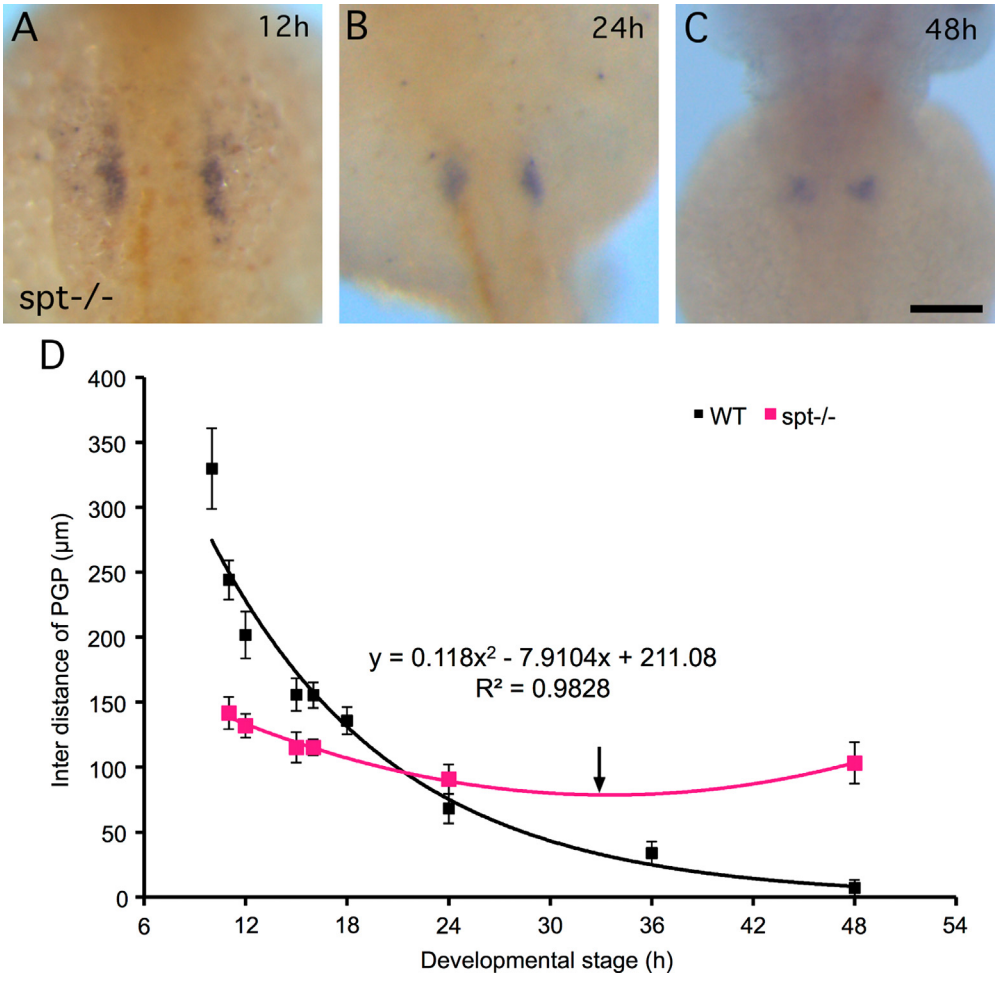

Fig. 6. PGP midline convergence phenotypes in $spt^{-/-}$ embryos. ((A)–(C)) Whole-mount *in situ* hybridization of *wt1a* and *myoD* was stained blue and orange, respectively in 12 (A), 24 (B) and 48 hpf (C) $spt^{-/-}$ embryos. The scale bar indicates 100 μm; ((A)–(C)) are at the same magnification. All images are dorsal view anterior to the top. (D) Quantification of convergence morphogenetic movements in $spt^{-/-}$ embryos and comparison with WT. The inter distance of PGP was measured at 11 (n=28), 12 (n=32), 15 (n=31), 24 (n=9), 48 (n=15) hpf. The P values of t-test for all 5 stages are smaller than 0.005. The curve fitting (pink) and R-squared value are displayed on the right-hand corner. A turning point (arrow) to divergence movement at 33.5 hpf is generated from an approximation of the stage that has the minimum inter distance of PGP. Error bars represent SD.

intersect in the formation of mesodermal tissues (Griffin and Kimelman, 2002; Schier et al., 1997). *Spt*, *oep* and *ntl* mutants exhibit effects on PGP convergence at the specification, coalescence and fusion steps, respectively. We conclude that all three genes *oep*, *ntl* and *spt* are essential for PGP midline convergence and play important roles in sequence in the progression of the convergence.

Tissue absence in mutant embryos

The inter PGP distance measurements generated from WT embryos are made in the context of normal organisation of the surrounding tissues (Supplementary, Fig. S1), whereas $zoep^{-/-}$, $spt^{-/-}$, *and* $ntl^{-/-}$ have defects in the formation of endodermal tissues, somites, and notochord, respectively (Ho and Kane, 1990; Molven et al., 1990; Odenthal et al., 1996a; Schier et al., 1997). According to our whole mount *in situ* results, the depletion or absence of endodermal tissues or notochord in $Zoep^{-/-}$ or $ntl^{-/-}$ did not result in changes in the dimensions of the bilateral PGP (Fig. 3F, Fig. 5D). However, these same mutants exhibited less tightly regulated PGP positions ($Zoep^{-/-}$) and reduced convergence after 24 hpf ($Zoep^{-/-}$, $ntl^{-/-}$). Somite formation had a major effect on inter-PGP distance in contrast to endodermal tissues or notochord formation. Inter-PGP distance is much smaller in $spt^{-/-}$ than in WT embryos at 12 hpf due to the absence of somite structure (Fig. 6A and D). Unlike $oep^{-/-}$ and $ntl^{-/-}$ results, which fit the WT formula well at early stages, PGP distances in $spt^{-/-}$ at 11, 12, and 15 hpf lay far below the WT curve (Fig. 6D). Nevertheless, the specification of wt1a expressing cells appears normal in double mutants of $Zoep^{-/-}$ and $ntl^{-/-}$ that lack somite marker expression (Schier et al., 1997; Weidinger et al., 2002). The mechanism for the specification of intermediate mesoderm is therefore not dependent on the formation of paraxial mesoderm. Notably, the mutants we have investigated also exhibit impaired circulation (data not shown), a known cause for defective midline migration in *isl, vtn* and *sih* mutants (Serluca et al., 2002).

Morphogenetic phenotypes are the outcome of collective cellular behavior

Wt1a is not only expressed in PGP but also in pronephric tubule progeny according to a previous cell lineage tracing study (Serluca and Fishman, 2001). The three genetic factors important for PGP midline convergence, *oep*, *spt* and *ntl*, relate to different cellular mechanisms, the pathways of which intersect in the formation of mesodermal tissues (Griffin and Kimelman, 2002; Schier et al., 1997). These mechanisms also include cell motility components and cell context effects that could influence PGP convergence.

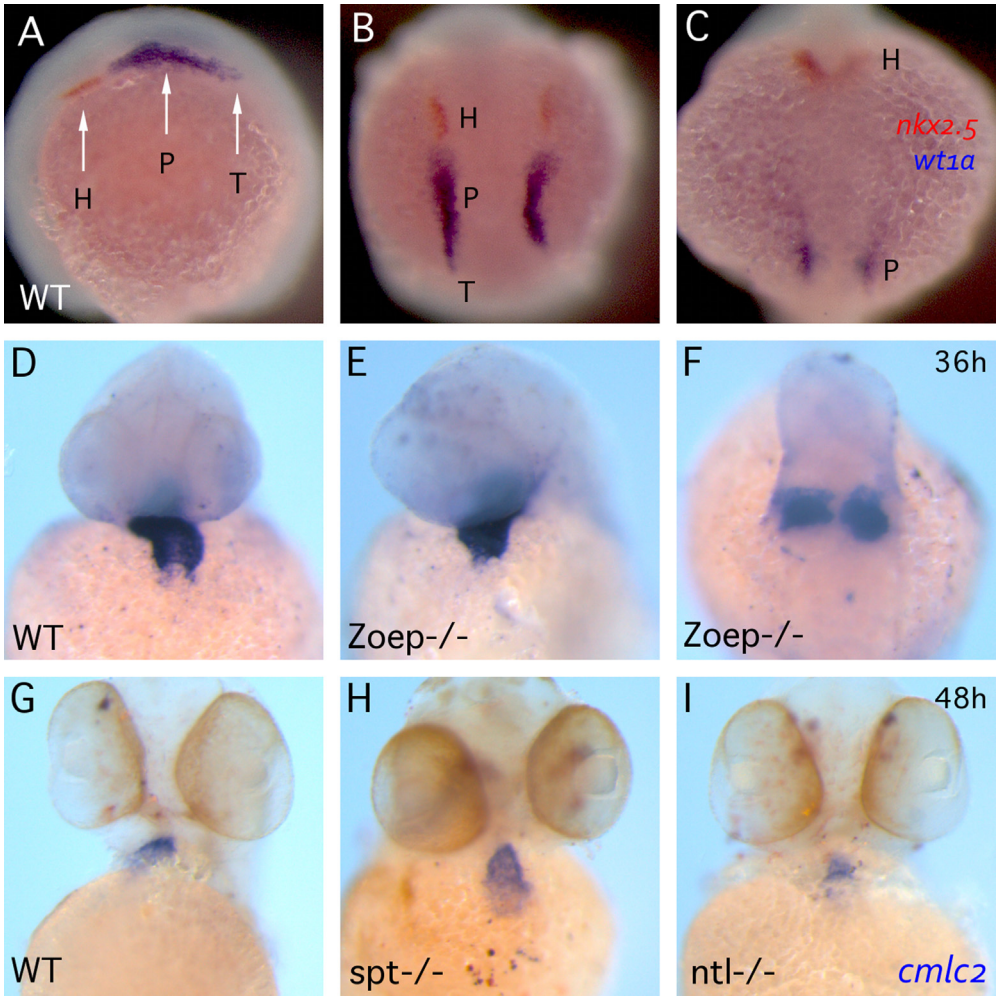

Fig. 7. PGP and cardiac midline convergence. ((A)–(C)) Transiency of PGP neighboring tissue. Double *in situ* of *nkx2.5* (orange) and *wt1a* (blue) at 12 ((A)–(B)) and 18 hpf (C). (A) The image is lateral view anterior to the right. ((B)–(C)) are dorsal view anterior to the top and same magnification. (H) heart primordium; (P) pronephric glomerular primordium; (T) tubule primordium. ((D)–(I)) Whole-mount *in situ* hybridization of *cmlc2* demonstrating cardiac morphogenetic phenotypes at 36 ((D)–(F)) and 48 hpf ((G)–(I)) in WT ((D) and (G)), *Zoep*$^{-/-}$ ((E) and (F)), *spt*$^{-/-}$ (H) and *ntl*$^{-/-}$ (I) embryos. ((D)–(I)) The images are same magnification and anterior to the top; ((A) and (B), (D)–(F)) are ventral view and (C) is dorsal view.

Zoep mutants show impaired cell-autonomous gastrulation movements due to increased cell cohesion separate from Nodal signaling defects (Wagner et al., 2003). *Spt* mutants lack the cell adhesion molecule paraxial protocadherin and show additional somitic mesodermal maturation timing defects (Griffin and Kimelman, 2002; Schier et al., 1997). *Wt1a* expressing cells in *oep*, *spt* and *ntl* mutant embryos are nevertheless as coherent as WT (Figs. 1D–G, Figs. 3A and B, Figs. 5A and B, Figs. 6A and B) and how these mutations affect PGP remains to be determined. Our study shows that quantification of PGP distance over developmental time can describe the morphogenetic changes of PG comprehensively, despite kidney development consisting of complicated cellular mechanisms. This quantitative approach will be of value in unravelling these mechanisms using mutants and knockdown strategies for gene manipulation.

The relative timing of pathway activation has long been thought a critical aspect in embryogenesis (Aulehla and Pourquie, 2008; Lewis, 2008). Theoretically, experiments with conditional knockdown (Hakamata and Kobayashi, 2010) of the relevant regulatory molecules at different time points would provide information on when these factors are involved in the process of PGP convergence. However to establish such experimental systems for every complex problem remains challenging. Here, we have applied simple quantitation of the morphogenetic changes to allow more refined analysis of the distinctive phases of cell movement during pronephros formation. Using this approach we were able to identify the distinctive temporal effects of *oep*, *spt* and *ntl* on PGP midline convergence consistent with a simple model (Supplementary, Fig. S2).

Acknowledgements

We thank Matthew Bailey and members of the Molecular Physiology Laboratory for discussions; Carl Tucker and Patricia Smart for fish care. Many thanks to Chih-Ying Su, MCDB, Yale University, for comments on the manuscript; Gaeriel Musso, Brigham and Women's Hospital and Harvard Medical School for helping with statistical analysis. Many thanks to the Zebrafish Facility in the MRC Centre for DBG at the University of Sheffield for providing the zebrafish *oep*, *spt* and *ntl* mutant alleles. Dr. Huang was supported by the Wellcome Trust 4-Year PhD program (Grant number: 076259/Z/04/A). The research program was also supported by the BHF Research Excellence Award.

Appendix A. Supporting information

Supplementary data associated with this article can be found in the online version at http://dx.doi.org/10.1016/j.ydbio.2013.07.002.

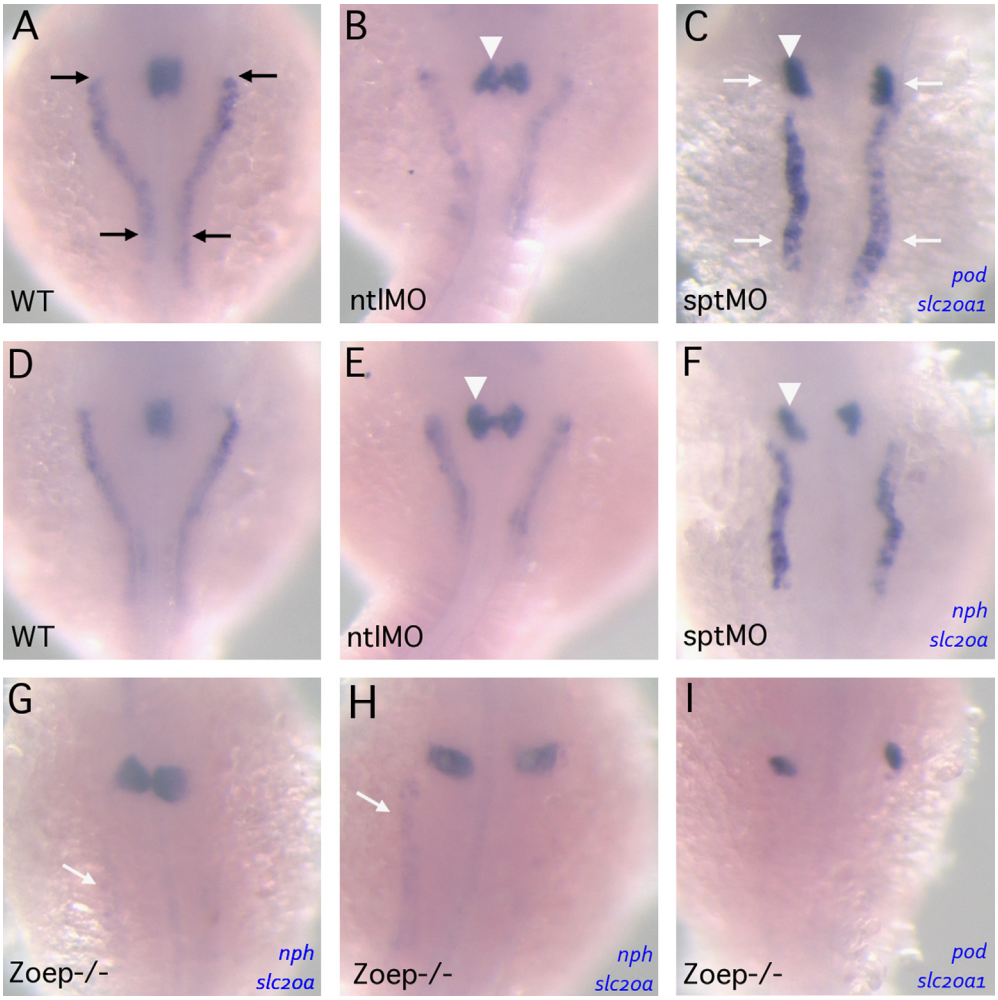

Fig. 8. Proximal convoluted tubules and PGP differentiation. Double *in situ* of *pod* and *slc20a1* ((A)–(C) and (I)) or *nph* and *slc20a1* ((D)–(H)) in WT ((A) and (D)), *ntl* morphant ((B) and (E)), *spt* morphant ((C) and (F)), Zoep$^{-/-}$ embryos ((G)–(I)) at 48 hpf. Arrows indicate proximal convolute tubules and arrowheads indicate PGP. All images are dorsal view anterior to the top and same magnification.

References

Altschmied, J., Hornung, U., Schlupp, I., Gadau, J., Kolb, R., Schartl, M., 1997. Isolation of DNA suitable for PCR for field and laboratory work. Biotechniques 23, 228–229.

Amacher, S.L., Kimmel, C.B., 1998. Promoting notochord fate and repressing muscle development in zebrafish axial mesoderm. Development 125, 1397–1406.

Amsterdam, A., Nissen, R.M., Sun, Z., Swindell, E.C., Farrington, S., Hopkins, N., 2004. Identification of 315 genes essential for early zebrafish development. Proc. Nat. Acad. Sci. U.S.A. 101, 12792–12797.

Aulehla, A., Pourquie, O., 2008. Oscillating signaling pathways during embryonic development. Curr. Opin. Cell Biol. 20, 632–637.

Bollig, F., Mehringer, R., Perner, B., Hartung, C., Schafer, M., Schartl, M., Volff, J.N., Winkler, C., Englert, C., 2006. Identification and comparative expression analysis of a second wt1 gene in zebrafish. Dev. Dyn. 235, 554–561.

Bouchard, M., Souabni, A., Mandler, M., Neubuser, A., Busslinger, M., 2002. Nephric lineage specification by Pax2 and Pax8. Genes Dev. 16, 2958–2970.

Drummond, I., 2003. Making a zebrafish kidney: a tale of two tubes. Trends Cell Biol. 13, 357–365.

Drummond, I.A., Majumdar, A., Hentschel, H., Elger, M., Solnica-Krezel, L., Schier, A. F., Neuhauss, S.C., Stemple, D.L., Zwartkruis, F., Rangini, Z., et al., 1998. Early development of the zebrafish pronephros and analysis of mutations affecting pronephric function. Development 125, 4655–4667.

Feldman, B., Dougan, S.T., Schier, A.F., Talbot, W.S., 2000. Nodal-related signals establish mesendodermal fate and trunk neural identity in zebrafish. Curr. Biol. 10, 531–534.

Feldman, B., Gates, M.A., Egan, E.S., Dougan, S.T., Rennebeck, G., Sirotkin, H.I., Schier, A.F., Talbot, W.S., 1998. Zebrafish organizer development and germ-layer formation require nodal-related signals. Nature 395, 181–185.

Griffin, K.J., Amacher, S.L., Kimmel, C.B., Kimelman, D., 1998. Molecular identification of spadetail: regulation of zebrafish trunk and tail mesoderm formation by T-box genes. Development 125, 3379–3388.

Griffin, K.J., Kimelman, D., 2002. One-Eyed Pinhead and Spadetail are essential for heart and somite formation. Nat. Cell Biol. 4, 821–825.

Gritsman, K., Zhang, J., Cheng, S., Heckscher, E., Talbot, W.S., Schier, A.F., 1999. The EGF-CFC protein one-eyed pinhead is essential for nodal signaling. Cell 97, 121–132.

Haffter, P., Granato, M., Brand, M., Mullins, M.C., Hammerschmidt, M., Kane, D.A., Odenthal, J., van Eeden, F.J., Jiang, Y.J., Heisenberg, C.P., et al., 1996. The identification of genes with unique and essential functions in the development of the zebrafish, Danio rerio. Development 123, 1–36.

Hakamata, Y., Kobayashi, E., 2010. Inducible and conditional promoter systems to generate transgenic animals. Methods Mol. Biol. 597, 71–79.

Hall, C., Flores, M.V., Storm, T., Crosier, K., Crosier, P., 2007. The zebrafish lysozyme C promoter drives myeloid-specific expression in transgenic fish. BMC Dev. Biol. 7, 42.

Ho, R.K., Kane, D.A., 1990. Cell-autonomous action of zebrafish spt-1 mutation in specific mesodermal precursors. Nature 348, 728–730.

Hong, S.K., Haldin, C.E., Lawson, N.D., Weinstein, B.M., Dawid, I.B., Hukriede, N.A., 2005. The zebrafish kohtalo/trap230 gene is required for the development of the brain, neural crest, and pronephric kidney. Proc. Nat. Acad. Sci. U.S.A. 102, 18473–18478.

Hsu, H.J., Lin, G., Chung, B.C., 2003. Parallel early development of zebrafish interrenal glands and pronephros: differential control by wt1 and ff1b. Development 130, 2107–2116.

Jowett, T., 2001. Double *in situ* hybridization techniques in zebrafish. Methods 23, 345–358.

Kimmel, C.B., Ballard, W.W., Kimmel, S.R., Ullmann, B., Schilling, T.F., 1995. Stages of embryonic development of the zebrafish. Dev. Dyn. 203, 253–310.

Kimmel, C.B., Kane, D.A., Walker, C., Warga, R.M., Rothman, M.B., 1989. A mutation that changes cell movement and cell fate in the zebrafish embryo. Nature 337, 358–362.

Kramer-Zucker, A.G., Wiessner, S., Jensen, A.M., Drummond, I.A., 2005. Organization of the pronephric filtration apparatus in zebrafish requires Nephrin, Podocin and the FERM domain protein Mosaic eyes. Dev. Biol. 285, 316–329.

Lewis, J., 2008. From signals to patterns: space, time, and mathematics in developmental biology. Science 322, 399–403.
Lewis, K.E., Eisen, J.S., 2004. Paraxial mesoderm specifies zebrafish primary motoneuron subtype identity. Development 131, 891–902.
Liu, A., Majumdar, A., Schauerte, H.E., Haffter, P., Drummond, I.A., 2000. Zebrafish wnt4b expression in the floor plate is altered in sonic hedgehog and gli-2 mutants. Mech. Dev. 91, 409–413.
Majumdar, A., Drummond, I.A., 2000. The zebrafish floating head mutant demonstrates podocytes play an important role in directing glomerular differentiation. Dev. Biol. 222, 147–157.
Matsui, T., Raya, A., Kawakami, Y., Callol-Massot, C., Capdevila, J., Rodriguez-Esteban, C., Izpisua Belmonte, J.C., 2005. Noncanonical Wnt signaling regulates midline convergence of organ primordia during zebrafish development. Genes Dev. 19, 164–175.
Molven, A., Wright, C.V., Bremiller, R., De Robertis, E.M., Kimmel, C.B., 1990. Expression of a homeobox gene product in normal and mutant zebrafish embryos: evolution of the tetrapod body plan. Development 109, 279–288.
Nasevicius, A., Ekker, S.C., 2000. Effective targeted gene 'knockdown' in zebrafish. Nat. Genet. 26, 216–220.
Nilius, B., Owsianik, G., Voets, T., Peters, J.A., 2007. Transient receptor potential cation channels in disease. Physiol. Rev. 87, 165–217.
O'Brien, J., Buckley, O., Doody, O., Ward, E., Persaud, T., Torreggiani, W., 2008. Imaging of horseshoe kidneys and their complications. J. Med. Imag. Radiat. Oncol. 52, 216–226.
Ober, E.A., Olofsson, B., Makinen, T., Jin, S.W., Shoji, W., Koh, G.Y., Alitalo, K., Stainier, D.Y., 2004. Vegfc is required for vascular development and endoderm morphogenesis in zebrafish. EMBO Rep. 5, 78–84.
Odenthal, J., Haffter, P., Vogelsang, E., Brand, M., van Eeden, F.J., Furutani-Seiki, M., Granato, M., Hammerschmidt, M., Heisenberg, C.P., Jiang, Y.J., et al., 1996a. Mutations affecting the formation of the notochord in the zebrafish, *Danio rerio*. Development 123, 103–115.
Odenthal, J., Rossnagel, K., Haffter, P., Kelsh, R.N., Vogelsang, E., Brand, M., van Eeden, F.J., Furutani-Seiki, M., Granato, M., Hammerschmidt, M., et al., 1996b. Mutations affecting xanthophore pigmentation in the zebrafish, *Danio rerio*. Development 123, 391–398.
Oktem, H., Gozil, R., Calguner, E., Bahcelioglu, M., Mutlu, S., Kurkcuoglu, A., Yucel, D., Senol, E., Babus, T., Kadioglu, D., 2008. Morphometric study of a horseshoe kidney. Med. Princ. Pract. 17, 80–83.
Perner, B., Englert, C., Bollig, F., 2007. The Wilms tumor genes wt1a and wt1b control different steps during formation of the zebrafish pronephros. Dev. Biol. 309, 87–96.
Rackley, R.R., Flenniken, A.M., Kuriyan, N.P., Kessler, P.M., Stoler, M.H., Williams, B. R., 1993. Expression of the Wilms' tumor suppressor gene WT1 during mouse embryogenesis. Cell Growth Differ. 4, 1023–1031.
Sakaguchi, T., Kikuchi, Y., Kuroiwa, A., Takeda, H., Stainier, D.Y., 2006. The yolk syncytial layer regulates myocardial migration by influencing extracellular matrix assembly in zebrafish. Development 133, 4063–4072.
Schafer, M., Rembold, M., Wittbrodt, J., Schartl, M., Winkler, C., 2005. Medial floor plate formation in zebrafish consists of two phases and requires trunk-derived Midkine-a. Genes Dev. 19, 897–902.
Schier, A.F., Neuhauss, S.C., Helde, K.A., Talbot, W.S., Driever, W., 1997. The one-eyed pinhead gene functions in mesoderm and endoderm formation in zebrafish and interacts with no tail. Development 124, 327–342.
Schier, A.F., Shen, M.M., 2000. Nodal signalling in vertebrate development. Nature 403, 385–389.
Schulte-Merker, S., van Eeden, F.J., Halpern, M.E., Kimmel, C.B., Nusslein-Volhard, C., 1994. no tail (ntl) is the zebrafish homologue of the mouse T (Brachyury) gene. Development 120, 1009–1015.
Serluca, F.C., Drummond, I.A., Fishman, M.C., 2002. Endothelial signaling in kidney morphogenesis: a role for hemodynamic forces. Curr. Biol. 12, 492–497.
Serluca, F.C., Fishman, M.C., 2001. Pre-pattern in the pronephric kidney field of zebrafish. Development 128, 2233–2241.
Shen, M.M., Schier, A.F., 2000. The EGF-CFC gene family in vertebrate development. Trends Genet. 16, 303–309.
Wagner, K.D., Wagner, N., Schedl, A., 2003. The complex life of WT1. J. Cell Sci. 116, 1653–1658.
Weidinger, G., Wolke, U., Koprunner, M., Thisse, C., Thisse, B., Raz, E., 2002. Regulation of zebrafish primordial germ cell migration by attraction towards an intermediate target. Development 129, 25–36.
Weinberg, E.S., Allende, M.L., Kelly, C.S., Abdelhamid, A., Murakami, T., Andermann, P., Doerre, O.G., Grunwald, D.J., Riggleman, B., 1996. Developmental regulation of zebrafish MyoD in wild-type, no tail and spadetail embryos. Development 122, 271–280.
Westerfield, M., 1995. The Zebrafish Book. University of Oregon Press, Eugene, Oregon.
Wingert, R.A., Davidson, A.J., 2008. The zebrafish pronephros: a model to study nephron segmentation. Kidney Int 73, 1120–1127.
Yamamoto, A., Amacher, S.L., Kim, S.H., Geissert, D., Kimmel, C.B., De Robertis, E.M., 1998. Zebrafish paraxial protocadherin is a downstream target of spadetail involved in morphogenesis of gastrula mesoderm. Development 125, 3389–3397.
Yeo, C., Whitman, M., 2001. Nodal signals to Smads through Cripto-dependent and Cripto-independent mechanisms. Mol. Cell. 7, 949–957.
Zhang, J., Talbot, W.S., Schier, A.F., 1998. Positional cloning identifies zebrafish one-eyed pinhead as a permissive EGF-related ligand required during gastrulation. Cell 92, 241–251.